

Planar Hall effect in c-axis textured films of $\text{Bi}_{85}\text{Sb}_{15}$ topological insulator

Cite as: AIP Advances **11**, 055020 (2021); <https://doi.org/10.1063/5.0049577>

Submitted: 06 March 2021 . Accepted: 03 May 2021 . Published Online: 14 May 2021

 Ramesh C. Budhani,  Joshua S. Higgins, Deandre McAlmont, and Johnpierre Paglione

COLLECTIONS

Paper published as part of the special topic on [Chemical Physics](#), [Energy, Fluids and Plasmas](#), [Materials Science](#) and [Mathematical Physics](#)



View Online



Export Citation



CrossMark



Call For Papers!

AIP Advances

SPECIAL TOPIC: Advances in
Low Dimensional and 2D Materials

Planar Hall effect in c-axis textured films of $\text{Bi}_{85}\text{Sb}_{15}$ topological insulator

Cite as: AIP Advances 11, 055020 (2021); doi: 10.1063/5.0049577

Submitted: 6 March 2021 • Accepted: 3 May 2021 •

Published Online: 14 May 2021



View Online



Export Citation



CrossMark

Ramesh C. Budhani,^{1,2,a)}  Joshua S. Higgins,²  Deandre McAlmont,¹ and Johnpierre Paglione²

AFFILIATIONS

¹Department of Physics, Morgan State University, Baltimore, Maryland 21251, USA

²Maryland Quantum Materials Center and Department of Physics, University of Maryland, College Park, Maryland 20742, USA

^{a)}Author to whom correspondence should be addressed: ramesh.budhani@morgan.edu

ABSTRACT

Measurements of the planar Hall effect (PHE) and anisotropic magnetoresistance (AMR) in polycrystalline films of topological insulator $\text{Bi}_{85}\text{Sb}_{15}$ are reported. The observation of PHE and AMR in these films of carrier density $\approx 2 \times 10^{19}$ electrons/cm³ is like the behavior of in-plane field transport in thin films of metallic ferromagnets. However, the amplitudes of PHE ($\Delta\rho^{\text{PHE}}$) and AMR ($\Delta\rho_{xx}$) are at variance. $\Delta\rho^{\text{PHE}}$ and $\Delta\rho_{xx}$ also undergo a sign reversal near ≈ 160 K. We compare these results with the reported PHE of topological insulators and Weyl semimetals and discuss possible scenarios for anisotropic backscattering of charge carriers in this non-magnetic alloy.

© 2021 Author(s). All article content, except where otherwise noted, is licensed under a Creative Commons Attribution (CC BY) license (<http://creativecommons.org/licenses/by/4.0/>). <https://doi.org/10.1063/5.0049577>

I. INTRODUCTION

Bismuth–antimony alloys ($\text{Bi}_{1-x}\text{Sb}_x$) are well-known thermoelectric (TE) materials.^{1,2} Their TE characteristics emanate from a tunable electronic band structure achieved by adjusting the Bi/Sb ratio in the alloy. This material has attracted much attention in recent years on the recognition of a strong spin–orbit interaction (SOI) driven band crossing in the composition range of $0.03 < x < 0.22$.^{3,4} For $x \approx 0.03$, it acquires a Dirac-like metallic state, which changes to a 3D Weyl semimetal on application of a magnetic field, with signatures of the chiral anomaly in longitudinal magnetoresistance (LMR).⁵ For $0.09 < x < 0.22$, ($\text{Bi}_{1-x}\text{Sb}_x$) is a 3D topological insulator (TI), as established by angle resolved photoemission measurements on single crystals⁶ and epitaxial thin films.⁷ Electronic transport measurements on such crystals are characterized by a metal-like resistivity at low temperatures and the presence of weak Shubnikov–de Haas oscillations in the magnetic field dependence of longitudinal (ρ_{xx}) and Hall (ρ_{xy}) resistivity.⁸ These features of electronic transport have been attributed to spin–momentum locked surface states. However, counter arguments suggesting subtle changes in bulk conduction at lower temperatures due to improved coherence and effectiveness of inadvertent doping have been given as well. The low effective mass of charge carriers and large dielectric function of $\text{Bi}_{1-x}\text{Sb}_x$ make the impurity conduction dominant

at low temperatures.⁹ The topological phase of ($\text{Bi}_{1-x}\text{Sb}_x$) has been identified as an excellent spin–orbit torque (SOT) material for spintronic applications.^{10–13} In epitaxial bilayers of BiSb and a ferromagnet (FM) like MnGa, the spin–momentum locked surface states of the former pump a large spin current into the FM layer under the action of a charge current driven Rashba–Edelstein effect (REE).¹⁴ The REE torque on the magnetization of the FM layer has been established to be much larger than the spin Hall effect driven torque of a heavy metal like Pt. Interestingly, two recent studies^{10,15} have indicated that the polycrystalline films of $\text{Bi}_{1-x}\text{Sb}_x$ made by a scalable process like sputtering are quite effective in producing spin currents to torque the magnetization of FeMn, FeCoB, and CoTb thin films. These observations have motivated us to undertake a detailed study of electronic transport in sputter-deposited polycrystalline films of BiSb. Although polycrystalline films of ($\text{Bi}_{1-x}\text{Sb}_x$) alloys have been studied previously by a number of groups,^{16–18} the focus of those studies has been their applicability as a thermoelectric material. Our objective here is to compare the low temperature ($T \geq 2$ K) magnetotransport in polycrystalline films of $\text{Bi}_{85}\text{Sb}_{15}$ with that of epitaxial films and single crystals where the existence of a topological phase has been established. We also seek to find the existence of the planar Hall effect (PHE) and anisotropic magnetoresistance (AMR), which have been seen earlier in several non-magnetic topological insulators^{19–24} and the Dirac/Weyl family of semimetals.^{25–28}

II. EXPERIMENTAL DETAILS

$\text{Bi}_{85}\text{Sb}_{15}$ films were deposited on thermally oxidized silicon wafers by magnetron sputtering of a stoichiometric 2-in. diameter alloy target in a laser deposition/sputtering hybrid load-lock chamber with a base pressure of $\sim 7 \times 10^{-8}$ Torr. The $\text{Bi}_{85}\text{Sb}_{15}$ alloy has a low melting temperature ($T_m \sim 300^\circ\text{C}$)²⁹ and high sputtering yield.³⁰ The sputter gun was operated at low power (≈ 25 W) to avoid surface melting of the target and to ensure a low growth rate (~ 0.15 nm/s). Films were deposited at ambient temperature and at 100 and 150 °C. It was noticed that the higher deposition temperature and excessive growth rates result in rough films. This is a perennial issue with the growth of thin films of low melting point alloys and elements.³⁰ The crystallographic structure of these films has been evaluated with x-ray diffraction. For measurements of magneto-transport, films were deposited through a shadow mask in a Hall bar geometry with the bar dimensions of $300 \times 3000 \mu\text{m}^2$. Transport measurements were carried out in a physical property measurement system in the temperature and field ranges of 2–300 K and 0 to ± 9 T, respectively. The use of a vertical sample rotator allowed in-plane and out-of-plane rotation of the film for measurements of anisotropic magnetoresistance and planar Hall effect.

III. RESULTS

The binary equilibrium phase diagram of $(\text{Bi}_{1-x}\text{Sb}_x)$ shows complete solubility of the two elements for all values of x , leading to a single-phase material of rhombohedral structure.³¹ However, due to the low melting points of Bi and Sb, the growth or annealing of BiSb films at $T > T_{\text{Liquidus}}$ may result in phase separation; therefore, we have deposited the films at only $T < 150^\circ\text{C}$. Figure 1 compares the Θ - 2Θ x-ray diffraction profiles of the two films grown at 35 and 100 °C. The x-ray profile of the film deposited at 35 °C shows diffraction peaks corresponding to several allowed hkl -indices with (001) reflections being most prominent. The higher intensity of such reflections suggests a predominantly c -axis oriented growth along the c -axis of the rhombohedral cell. This preferential growth

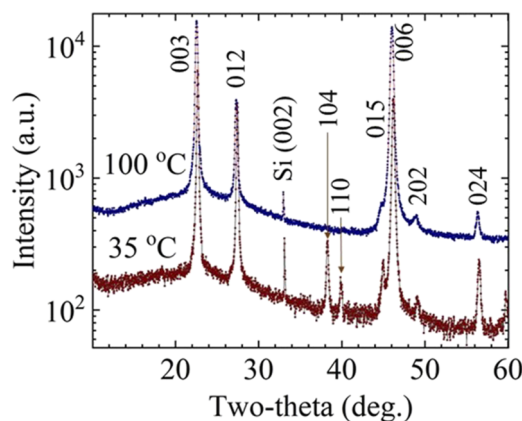


FIG. 1. X-ray diffraction profile of the $\text{Bi}_{85}\text{Sb}_{15}$ thin film deposited on thermally oxidized silicon at 35 and 100 °C. The diffraction peaks have been indexed for the Miller indices of the rhombohedral structure of the BiSb alloy. A preferred orientation of the film along the c -axis is evident in these data.

becomes prominent at 100 °C as indicated by the suppression of the intensity of reflections corresponding to non-zero values of h and k indices. These observations are consistent with the results of Rochford *et al.*¹⁶ on $\text{Bi}_{80}\text{Sb}_{20}$ films deposited on thermally oxidized silicon by cosputtering of elemental targets. Films of $\text{Bi}_{85}\text{Sb}_{15}$ deposited by radio frequency sputtering of the alloy target on (0001) sapphire reveal a preferential c -axis growth due to a better c -plane lattice match between sapphire and BiSb.³¹

Here, we focus on electron transport in the BiSb films deposited at $\approx 35^\circ\text{C}$. Ambient temperature growth of the TI film is preferred when it is deposited on amorphous ferromagnets like FeGaB, FeCoB, and Fe–Gd alloys to avoid their crystallization. The inset of Fig. 2 shows the zero-field longitudinal resistivity of the film between 2 and 300 K. The resistivity first rises on lowering the temperature down to ~ 180 K, and then, this rise tapers off, leading to a resistivity of ~ 2.0 m Ω cm at 2 K. This behavior of resistivity is comparable to that reported by Fan *et al.*³¹ for sputter-deposited films on (0001) sapphire.

It is also worth comparing the resistivity of these films with those made by molecular beam epitaxy. The data of Cho *et al.*² for films grown by MBE on CdTe crystals reveal a resistivity of ~ 0.2 m Ω cm at 300 K, which rises to ~ 2.5 m Ω cm at 2 K. While the resistivity ratio $\rho(2\text{ K})/\rho(300\text{ K})$ of the MBE grown films is the same (~ 1.2) as that of the sputter-deposited films reported here, the temperature dependence of resistivity is strikingly different in the two cases. The resistivity of sputtered polycrystalline films first rises and then tapers off, while for the MBE films,² the rise is faster at lower temperatures. Interestingly, the $\rho_{xx}(2\text{ K})/\rho_{xx}(300\text{ K})$ ratio for $\text{Bi}_{1-x}\text{Sb}_x$ single crystals with $x = 0.09$ is ≈ 1.8 ,⁸ with a $\rho_{xx}(300\text{ K})$ of ~ 0.16 m Ω cm. The temperature dependence of ρ_{xx} is similar to that of the sputtered film, barring some signatures of a metallic conduction at $T < 50$ K, which is presumably due to well-defined conducting surface states in single crystal samples.

The main panel of Fig. 2 shows the Hall resistivity (ρ_{xy}) of the ambient temperature deposited film measured between 2 and 20 K as a function of magnetic field. ρ_{xy} is linear in field for $\mu_0 H \leq 3$ T and does not show any temperature dependence. In the framework of a simple Drude model, it yields a carrier density of 1.97×10^{19} electrons/cm³ and carrier mobility of ~ 203 cm² V⁻¹ s⁻¹. The slight upward curvature of ρ_{xy} vs H at the higher fields suggests a

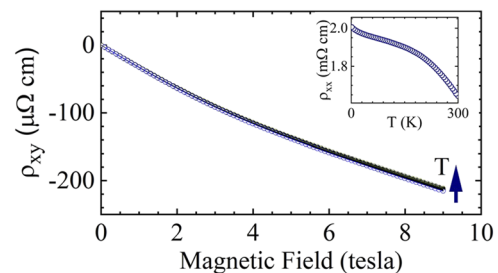


FIG. 2. Hall resistivity (ρ_{xy}) of the $\text{Bi}_{85}\text{Sb}_{15}$ film measured between 2 and 20 K as a function of magnetic field. The linear portion of ρ_{xy} vs $\mu_0 H$ has been used to calculate the carrier concentration. The Hall resistivity shows a very weak temperature dependence at high fields. The inset of the figure shows the resistivity (ρ_{xx}) of the film in zero-field measured between 2 and 300 K.

two-carrier scenario for electron transport in this system. The high field data also reveal a very weak temperature dependence in the temperature range of 2–20 K. While there is a lack of carrier concentration and mobility data on epitaxial and polycrystalline films of $\text{Bi}_{1-x}\text{Sb}_x$, the carrier concentration in our films is ~ 2 orders of magnitude higher than that reported by Taskin and Ando⁸ for $x = 0.09$ BiSb single crystals and the carrier mobility of these films is smaller by the same factor.

The measurements of the electrical resistivity of 3D topological insulators and Dirac/Weyl semimetals in a configuration where the current density, magnetic field, and induced electric field are in the same plane have generated considerable interest due to the presence of anisotropic magnetoresistance and planar Hall effect,^{19–28} which have traditionally been the signatures of electronic transport in a magnetically ordered metal.³² We carried out the measurements of the electrical resistivity of BiSb thin films in a field-in-plane geometry. Here, the transport current J_x ($=25 \text{ A/cm}^2$) flows in the x direction, and the induced electric fields E_{xx} and E_{xy} in the x and y directions, respectively, are measured as the magnetic field is rotated in the xy plane from -90° to 270° . The angle $\phi = 0$ corresponds to the situation where H and J_x are parallel. The induced electric field in the direction of J_x yields magnetoresistivity, whereas the orthogonal field E_{xy} results in the planar Hall effect.

The components of the resistivity tensor are expressed as^{20,32}

$$\rho_{xx} = \rho_{\perp} - \Delta\rho \cos^2 \phi, \quad (1)$$

$$\rho^{\text{PHE}} = -\Delta\rho \sin \phi \cos \phi, \quad (2)$$

where $\Delta\rho = \rho_{\perp} - \rho^{\parallel}$, with ρ_{\perp} and ρ^{\parallel} corresponding to H perpendicular to J_x and H parallel to J_x , respectively. The anisotropic magnetoresistance ($\Delta\rho$) and ρ^{PHE} are characteristic features of spin-orbit scattering dominated electronic transport in magnetic alloys due to

coexisting s and d bands near the Fermi energy.³² Interestingly, however, PHE and anisotropic magnetoresistance have been found in non-magnetic 3D topological insulators like Bi_2Te_3 and Bi_2Se_3 ,^{19–24} including the observation of a nonlinear response at higher current densities in epitaxial films of Bi_2Se_3 , which depends on the direction of current with respect to the crystal axis of the monolayer.^{23,24} Appreciable values of AMR and PHE have been observed in Dirac and Weyl semimetals as well.^{25–28} While in the latter class of semimetals, this anisotropic transport has been attributed to breaking of chiral symmetry, which results in a large negative longitudinal magnetoresistance (NLMR), varied interpretations have been proposed for PHE in 3D TIs where no NLMR is seen.

$\text{Bi}_{1-x}\text{Sb}_x$ is one of the first reported 3D TIs. While the measurements of the Hall resistivity and orbital MR in single crystals and epitaxial films of $\text{Bi}_{1-x}\text{Sb}_x$ have been reported earlier,^{6,8,9} data on PHE and AMR are lacking. Figure 3(a) shows the variation of ρ_{xx} and ρ_{xy} at 2 K and +9 T as the sample is rotated to change the angle between magnetic field and current density directions from -90° to 270° . A similar measurement of ρ_{xx} and ρ_{xy} at 2 K with the field direction reversed is shown in Fig. 3(b). We note that the positions of extrema in ρ_{xx} and ρ_{xy} data of Figs. 3(a) and 3(b) are consistent with Eqs. (1) and (2). However, there is a noticeable asymmetry in the behavior of ρ_{xy} for the two field orientations. There are two factors that contribute to this asymmetry. First is a normal Hall voltage that results from a non-zero out-of-plane component of the magnetic field due to a misalignment of the film plane and the plane of rotation. This contribution is antisymmetric in field and can be eliminated on symmetrization of the (+H) and (−H) data. Second is a zero-field misalignment voltage across the Hall contacts, which will add to the PHE voltage on symmetrization of ρ_{xy} [$\{(\rho_{xy}(+H) + \rho_{xy}(-H))/2\}$]. This constant resistance can be subtracted from the measured $\rho_{xy}(H)$ provided its value is small such that the AMR induced change in it is insignificant compared to the true $\rho_{xy}(H)$. In addition to these two factors, another contaminant of ρ_{xy} comes from the orbital

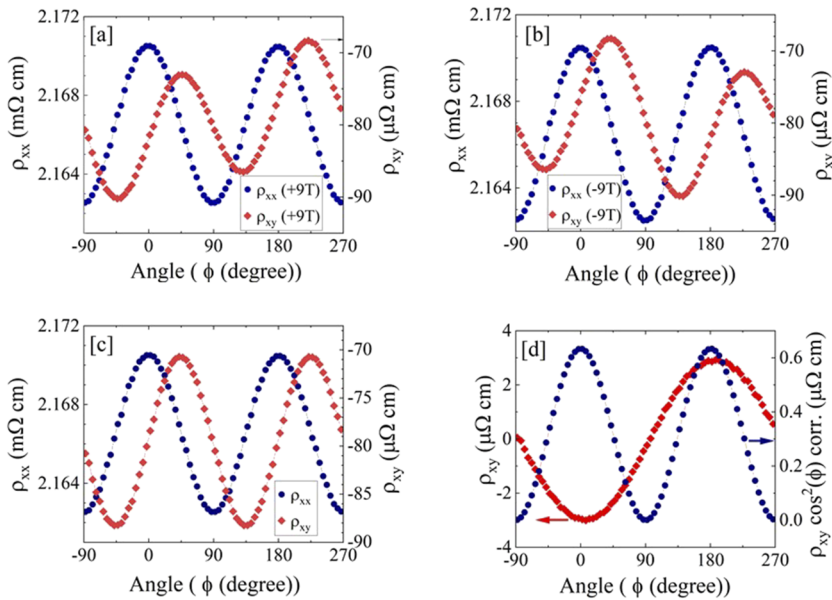


FIG. 3. The variation of ρ_{xx} and ρ_{xy} as a function of the angle (ϕ) between the direction of a 9 T field and the direction of current density J_x . (a) +9 T, (b) -9 T, and (c) ρ_{xx} and ρ_{xy} on symmetrization of the data shown in (a) and (b). The solid lines in (c) are fits to the equation of the type $\rho_{xx}(\phi) = \rho_{xx}(0) - \Delta\rho_{xx} \cos^2 \phi$ and $\rho_{xy}(\phi) = \rho_{xy}(0) - \Delta\rho_{xy} \sin \phi \cos \phi + B \cos^2(\phi)$ to the ρ_{xx} and ρ_{xy} data, respectively. (d) shows the variation of antisymmetric ρ_{xy} extracted from (a) and (b) and the variation of coefficient B extracted from the fit in (c).

magnetoresistance (OMR) of the misaligned section of the transverse contacts when the sample is tilted with respect to the plane of rotation. This would add a $\cos^2 \phi$ term in Eq. (2). The misalignment of the plane of rotation and the plane of the sample adds an error in the value of AMR as well. If the OMR of the sample is large, then the normal component of the field will add an OMR contribution to ρ_{xx}^{\perp} and ρ_{xx}^{\parallel} . We address these errors by first symmetrizing the $\rho_{xx}(\phi)$ and $\rho_{xy}(\phi)$ data of Figs. 3(a) and 3(b). The result of this procedure is displayed in Fig. 3(c), along with the fits of $\rho_{xx}(\phi)$ to Eq. (1) and of $\rho_{xy}(\phi)$ to a function of the type $\rho_{xy}(\phi) = A + B \sin(\phi) \cos(\phi) + C \cos^2(\phi)$. The last term of this equation considers the error in ρ_{xy} due to OMR of the misaligned section, as discussed earlier. The magnitude of this error [$C \cos^2(\phi)$] and the antisymmetric contribution to ρ_{xy} are displayed in Fig. 3(d). Comparing the peak amplitude of ρ_{xy} in Fig. 3(c) and the peak amplitude of the $C \cos^2(\phi)$ term in Fig. 3(d) shows that the maximum error introduced by this term in the measurement of ρ_{xy} is $\leq \pm 3.5\%$. Moreover, a comparison of

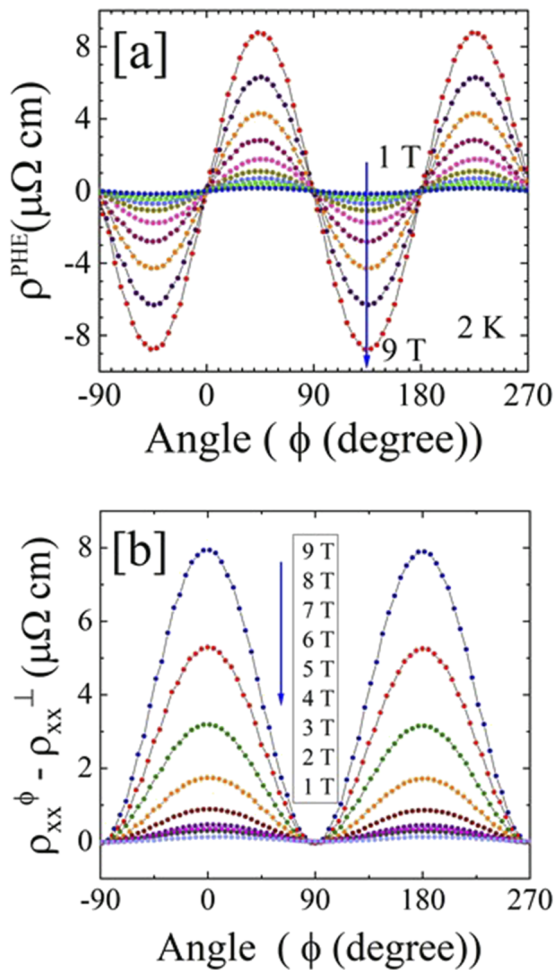


FIG. 4. The angle (ϕ) dependence of ρ^{PHE} and ρ_{xx} has been measured at 2 K for several values of magnetic field. (a) and (b) show the symmetrized ρ_{xy} and ρ_{xx} data as a function of angle.

the peak value of antisymmetric ρ_{xy} ($\approx 3 \mu\Omega \text{ cm}$) at 9 T in Fig. 3(d) with the Hall resistance data shown in Fig. 2 linearized in field (slope $\approx 70 \mu\Omega \text{ cm/T}$) yields a tilt angle of $\approx 0.6^\circ$ with respect to the plane of the sample. The angular dependencies of the symmetrized ρ_{xy} and ρ_{xx} at 2 K for several values of field are shown in Figs. 4(a) and 4(b), respectively. In the plot of Fig. 4(a), the constant offset value of $\Delta\rho_{xy}$ at zero-field has been subtracted, whereas Fig. 4(b) displays the variation of $\rho_{xx}(\phi)$ with respect to the average value of ρ_{xx} at $\phi = \pm 90^\circ$. The dominant $\sin(\phi) \cdot \cos(\phi)$ and $\cos^2(\phi)$ dependencies of these quantities are evident in Figs. 4(a) and 4(b), respectively. The variation of the peak amplitudes of $\Delta\rho^{\text{PHE}}$ and $\Delta\rho_{xx}$ ($\rho_{xx}^{\parallel} - \rho_{xx}^{\perp}$) extracted from these plots as a function of magnetic field is shown in Fig. 5. The two important conclusions that can be drawn from these data are: (1) the longitudinal magnetoresistance is positive with a field dependence of the type $\Delta\rho_{xx} \sim H^\alpha$ ($\alpha = 1.5$) and (2) the PHE amplitude is larger than $\Delta\rho_{xx}$.

In the inset of Fig. 5, we plot the variation of orbital magnetoresistance ($\Delta R^{\text{OMR}} = [(R_{xx}(H) - R_{xx}(0))/R_{xx}(0)] \times 100$) with field normal to the film plane, longitudinal magnetoresistance (LMR) ($\Delta R^{\text{LMR}} = [(R_{xx}^{\parallel}(H) - R_{xx}(0))/R_{xx}(0)] \times 100$) with field parallel (\parallel) to J_x , and anisotropic magnetoresistance ($\Delta R^{\text{AMR}} = [(R_{xx}^{\parallel}(H) - R_{xx}^{\perp}(H))/R_{xx}^{\perp}(H)] \times 100$). Two noteworthy conclusions that can be drawn from these data are: (1) the LMR is larger than OMR and (2) the AMR is small but positive, indicating the absence of any chiral anomaly.

The resistance tensor of a two-dimensional magnetic film for an in-plane magnetic field predicts that the amplitudes of $\Delta\rho^{\text{PHE}}$ and $\Delta\rho_{xx}$ should be the same. The large difference seen in the values of $\Delta\rho^{\text{PHE}}$ and $\Delta\rho_{xx}$ in this case points toward some subtle differences in the origin of these components in the resistance tensor. One might argue²⁰ that in systems with large orbital magnetoresistance, the out of film plane magnetic field due to sample misalignment may significantly change the value of $\Delta\rho_{xx}$. An estimation of this error can be made by looking at the results of the orbital MR measurements shown in Fig. 5 and the estimated tilt of 0.6° from the antisymmetric ρ_{xy} in Fig. 3(d). This much tilt at 9 T would result

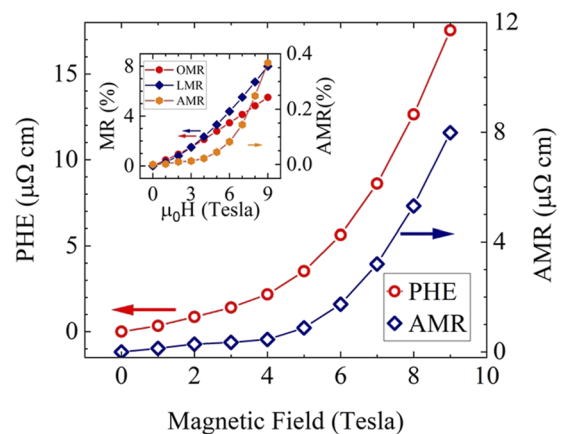


FIG. 5. Amplitudes of $\Delta\rho^{\text{PHE}}(\phi)$ and $\Delta\rho_{xx}(\phi)$ at 2 K plotted as a function of magnetic field. The inset shows the variation of out-of-plane and in-plane field magnetoresistance and anisotropic magnetoresistance as a function of applied field.

in a ≈ 95 mT perpendicular field. From Fig. 5, we conclude that the effect of this misalignment of field on the measurement of $\Delta\rho_{xx}$ is negligible.

We have also considered the possibility of contamination of $\Delta\rho_{xx}$ by the large thermoelectric power of BiSb alloys.^{1,2} This effect may get accentuated by the large distance (≈ 2000 μm) between the V_{xx} pads compared to the distance (≈ 300 μm) between V_{xy} pads if any thermal gradients across the length of the sample are produced by uneven cooling. However, this speculated thermoelectric contribution to the longitudinal voltage will lead to an asymmetry in V_{xx} at $\phi = 0^\circ$ and $\phi = 180^\circ$, which we do not see. Clearly, the difference in the amplitudes of $\Delta\rho_{xx}$ and $\Delta\rho_{xy}^{\text{PHE}}$ does not appear to be a spurious effect emerging from any misalignment or thermal gradients.

Figures 6(a) and 6(b), respectively, show the angular dependence of $\Delta\rho^{\text{PHE}}$ and $\Delta\rho_{xx}$ at several temperatures in the range of 10–160 K. A significant drop in the amplitude of PHE and AMR is seen on increasing the temperature, followed by a sign change in the temperature window of 150–200 K. The amplitudes of $\Delta\rho^{\text{PHE}}$ and

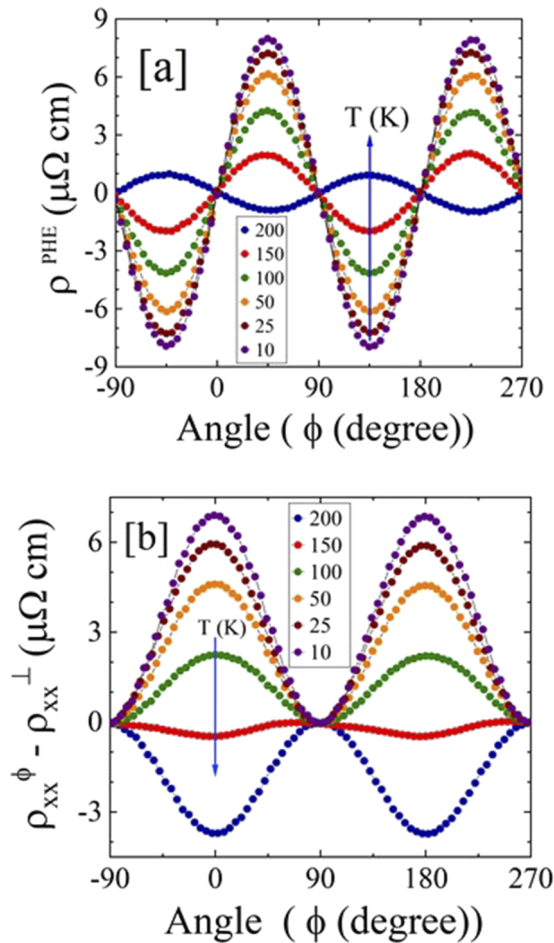


FIG. 6. Angle (ϕ) dependence of $\Delta\rho^{\text{PHE}}$ and $\Delta\rho_{xx}$ at several temperatures from 2 to 160 K is shown in (a) and (b), respectively. The data have been obtained by symmetrization of the plus and minus field response.

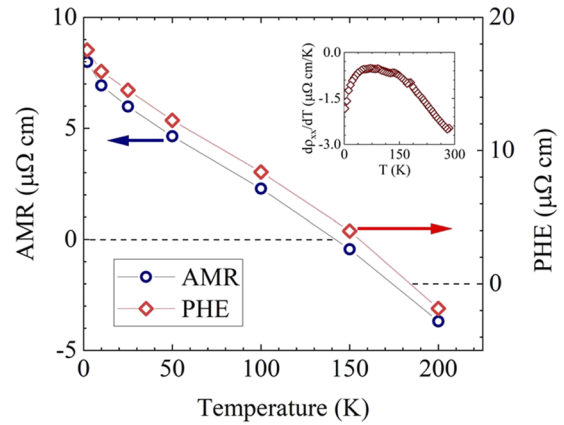


FIG. 7. Variation of the PHE amplitude [$\Delta\rho^{\text{PHE}}(\phi)$] and $\Delta\rho_{xx}(\phi)$ amplitude as a function of temperature. The inset of the figure shows $d\rho_{xx}/dT$ vs T in zero-field.

$\Delta\rho_{xx}$ are plotted in Fig. 7. The change in the sign of these two quantities appears to correlate with the inflection point in the temperature dependence of ρ_{xx} , as can be seen in the inset where we have plotted $d\rho_{xx}/dT$ vs T .

IV. DISCUSSION

The noteworthy features of the in-plane magnetoresistance of these $\text{Bi}_{85}\text{Sb}_{15}$ thin films are: (1) observation of a planar Hall effect, (2) a difference in the amplitudes of $\Delta\rho^{\text{PHE}}$ and $\Delta\rho_{xx}$, and (3) a sign reversal of these two quantities in the vicinity of 150 K. Although BiSb is non-magnetic, this first observation of PHE in BiSb is consistent with the recent reports of PHE in non-magnetic semimetals like $(\text{Bi}_{1-x}\text{Sb}_x)_2\text{Te}_3$,²⁰ bismuth,³¹ and MoTe_2 .^{25,26} with non-trivial band topology. The observation of PHE in $(\text{Bi}_{1-x}\text{Sb}_x)_2\text{Te}_3$ has been attributed to scattering by magnetic impurities present in the sample.²⁰ The anisotropy of the Fermi surface and the resulting large difference in the magnetic field dependence of ρ_{xx}^\perp and ρ_{xx}^\parallel have also been argued to be the source of PHE in some systems.^{26,33} We have analyzed the field dependence of ρ_{xx}^\perp and ρ_{xx}^\parallel at 2 K. The resistance rises as $\sim H^\alpha$, with α as 1.46 and 1.51 for the \perp and \parallel measurements, respectively. A treatment of electron transport in the framework of a semiclassical Boltzmann transport equation attributes PHE in topological insulators to orbital magnetism of Bloch electrons, which is non-zero because of the symmetry breaking in-plane magnetic field.^{22,27} This model, however, does not predict a difference in the value of $\Delta\rho^{\text{PHE}}$ and $\Delta\rho_{xx}$. The experimental data of Taskin *et al.*²⁰ on the $(\text{Bi}_{1-x}\text{Sb}_x)_2\text{Te}_3$ crystal show a large difference in ΔR^{PHE} and ΔR_{xx} , which the authors have attributed to a contamination of the signal by an OMR contribution arising from the misalignment of the sample plane and the plane of rotation. However, this scenario does not apply in the present case as we have shown that the difference in $\Delta\rho^{\text{PHE}}$ and $\Delta\rho_{xx}$ cannot be attributed to a tilt of the sample plane. Similarly, a change in the sign of planar Hall and anisotropic magnetoresistance at higher temperatures is difficult to explain based on misalignment and/or impurity scattering.

A plausible description of this difference in the amplitudes of $\Delta\rho^{\text{PHE}}$ and $\Delta\rho_{xx}$ as well as of the sign change has been given by

Zheng *et al.*²⁸ where they consider the tilt of Dirac cones in the TI induced by the in-plane magnetic field. This tilt contributes to anisotropic backscattering, which is enhanced further by impurity resonant states and may lead to a sign change in AMR. The change in the sign of AMR of our BiSb films is consistent with this picture.

V. CONCLUSIONS

In summary, we have addressed the behavior of longitudinal and Hall resistivities of highly oriented thin films of the Bi₈₅Sb₁₅ topological insulator, which has been established as a superior spin torque material for spintronic applications.^{11–15} The overall features of the out-of-plane magnetic field transport are comparable to earlier reports on MBE grown films. The in-plane field transport reveals a striking planar Hall effect whose magnitude is larger by a factor of ≈ 2 as compared to the magnitude of AMR. Moreover, both PHE and AMR undergo a sign change on raising the sample temperature beyond ~ 150 K. These new features of the in-plane magnetic field transport presumably arise due to anisotropic scattering of Dirac electrons in a planar magnetic field.

ACKNOWLEDGMENTS

This research was supported by the Air Force Office of Scientific Research, Grant No. FA9550-19-1-0082 awarded to Morgan State University. J.P. acknowledges support from the Gordon and Betty Moore Foundation's EPiQS Initiative through Grant No. GBMF9071, and J.S.H. acknowledges support from the National Institute of Standards and Technology Cooperative Agreement No. 70NANB17H301.

DATA AVAILABILITY

The data that support the findings of this study are available from the corresponding author upon reasonable request.

REFERENCES

- W. M. Yim and A. Amith, "Bi-Sb alloys for magneto-thermoelectric and thermomagnetic cooling," *Solid. State. Electron.* **15**, 1141 (1972).
- S. Cho, A. DiVenere, G. K. Wong, J. B. Ketterson, and J. R. Meyer, *Phys. Rev. B* **59**, 10691 (1999).
- J. C. Y. Teo, L. Fu, and C. L. Kane, *Phys. Rev. B* **78**, 045426 (2008).
- H. Guo, K. Sugawara, A. Takayama, S. Souma, T. Sato, N. Satoh, A. Ohnishi, M. Kitaura, M. Sasaki, Q.-K. Xue, and T. Takahashi, *Phys. Rev. B* **83**, 201104(R) (2011).
- D. Shin, Y. Lee, M. Sasaki, Y. H. Jeong, F. Weickert, J. B. Betts, H.-J. Kim, K.-S. Kim, and J. Kim, *Nat. Mater.* **16**, 1096 (2017).
- A. Nishide, A. A. Taskin, T. Yasuo, T. Okuda, A. Kakizaki, T. Hirahara, N. Kan, F. Komori, Y. Ando, and I. Matsuda, *Phys. Rev. B* **81**, 041309(R) (2010).
- T. Hirahara, Y. Sakamoto, Y. Saisyu, H. Miyazaki, S. Kimura, T. Okuda, I. Matsuda, S. Murakami, and S. Hasegawa, *Phys. Rev. B* **81**, 165422 (2010).
- A. A. Taskin and Y. Ando, *Phys. Rev. B* **80**, 085303 (2009).
- D. Minh Vu, W. Shon, J.-S. Rhyee, M. Sasaki, A. Ohnishi, K.-S. Kim, and H.-J. Kim, *Phys. Rev. B* **100**, 125162 (2019).
- Z. Chi, Y.-C. Lau, X. Xu, T. Ohkubo, K. Hono, and M. Hayashi, *Sci. Adv.* **6**, 2324 (2020).
- N. H. Duy Khang, Y. Ueda, K. Yao, and P. N. Hai, *J. Appl. Phys.* **122**, 143903 (2017).
- N. H. Duy Khang, Y. Ueda, and P. Nam Hai, *Nat. Mater.* **17**, 808 (2018).
- N. Roschewsky, E. S. Walker, P. Gowtham, S. Muschinske, F. Hellman, R. B. Seth, and S. Salahuddin, *Phys. Rev. B* **99**, 195103 (2019).
- F. Hellman *et al.*, *Rev. Mod. Phys.* **89**, 025006 (2017).
- N. H. Duy Khang, S. Nakano, T. Shirokura, Y. Miyamoto, and P. Nam Hai, *Sci. Rep.* **10**, 12185 (2020).
- C. Rochford, D. L. Medlin, K. J. Erickson, and M. P. Siegal, *APL Mater.* **3**, 126106 (2015).
- R. C. Mallik and V. D. Das, *J. Appl. Phys.* **98**, 023710 (2005).
- T. Massana, C. N. Afonso, A. K. Petford-long, and R. C. Doole, *Thin Solid Films* **288**, 186 (1996).
- S. Wiedmann, A. Jost, B. Fauque, J. van Dijk, M. J. Meijer, T. Khouri, P. Oezzini, S. Grauer, S. Schreyeck, C. Brune, H. Buhmann, L. W. Molenkamp, and N. E. Hussey, *Phys. Rev. B* **94**, 081302 (2016).
- A. A. Taskin, H. F. Legg, F. Yang, S. Sasaki, Y. Kanai, K. Matsumoto, A. Rosch, and Y. Ando, *Nat. Commun.* **8**, 1340 (2017).
- A. A. Burkov, *Phys. Rev. B* **96**, 041110 (2017).
- S. Nandy, A. Taraphder, and S. Tewari, *Sci. Rep.* **8**, 14983 (2018).
- P. He, S. S.-L. Zhang, D. Zhu, Y. Liu, Y. Wang, J. Yu, G. Vignale, and H. Yang, *Nat. Phys.* **14**, 495 (2018).
- P. He, S. S.-L. Zhang, D. Zhu, S. Shi, O. G. Heinonen, G. Vignale, and H. Yang, *Phys. Rev. Lett.* **123**, 016801 (2019).
- F. C. Chen, X. Luo, J. Yan, Y. Sun, H. Y. Lv, W. J. Lu, C. Y. Xi, P. Tong, Z. G. Sheng, X. B. Zhu, W. H. Song, and Y. P. Sun, *Phys. Rev. B* **98**, 041114(R) (2018).
- D. D. Liang, Y. J. Wang, W. L. Zhen, J. Yang, S. R. Weng, X. Yan, Y. Y. Han, W. Tong, W. K. Zhu, L. Pi, and C. J. Zhang, *AIP Adv.* **9**, 055015 (2019).
- S. Nandy, G. Sharma, A. Taraphder, and S. Tewari, *Phys. Rev. Lett.* **119**, 176804 (2017).
- S.-H. Zheng, H.-J. Duan, J.-K. Wang, J.-Y. Li, M.-X. Deng, and R.-Q. Wang, *Phys. Rev. B* **101**, 041408(R) (2020).
- H. Okamoto, *J. Phase Equilib. Diffus.* **33**, 493 (2012).
- Handbook of Sputter Deposition Technology*, 2nd ed., edited by K. Wasa, I. Kanno, and H. Kotera (Elsevier, 2012), p. 42.
- T. Fan, M. Tobah, T. Shirokura, N. Huynh Duy Khang, and P. Nam Hai, *Jpn. J. Appl. Phys., Part 1* **59**, 063001 (2020).
- I. A. Campbell, A. Fert, and O. Jaoul, *J. Phys. C: Solid State Phys.* **3**, S95 (1970).
- S.-Y. Yang, K. Chang, S. Stuart, and P. Parkin, *Phys. Rev. Res.* **2**, 022029(R) (2020).